# Photocatalytic degradation of sulfamethoxazole using $TiO_2$ in simulated seawater: evidence for direct formation of reactive halogen species and halogenated by-products

Oriol Porcar-Santos*, Alberto Cruz-Alcalde, Núria López-Vinent, Dimitrios Zanganas, Carme Sans

Department of Chemical Engineering and Analytical Chemistry, Faculty of Chemistry, Universitat de Barcelona, C/Martí i Franqués 1, 08028 Barcelona, Spain

*Corresponding author: oriol.porcar@ub.edu

**Keywords**: Titanium dioxide nanoparticles, saline water, photocatalysis, RHS, ROS, halogenation

---

**Abstract**

Nowadays photoactivation mechanism of titanium dioxide nanoparticles ($TiO_2$ NPs) and reactive species involved in saline waters is not sufficiently established. In this study, $TiO_2$ photocatalytic process under simulated solar irradiation was evaluated in synthetic seawater and compared with deionized water, using sulfamethoxazole (SMX) as model organic compound. For a $TiO_2$ concentration of 100 mg $L^{-1}$, SMX degradation resulted two times slower in seawater than in deionized water by the determination of their pseudo-first order rate constants of 0.020 $min^{-1}$ and 0.041 $min^{-1}$, respectively. Selected scavenging experiments revealed no significant contribution of hydroxyl radicals ($^{\bullet}OH$) on the degradation process in seawater, while these radicals contributed to circa 60% on the SMX depletion in deionized water. Instead, the involvement of reactive halogen species (RHS) as main contributors for the SMX degradation in seawater could be established. A mechanism for the RHS generation was proposed, whose initiation reactions involve halides with the $TiO_2$ photogenerated holes, yielding chlorine and bromine radicals ($Cl^{\bullet}$ and $Br^{\bullet}$) that may later generate other RHS. Production of RHS was further confirmed by the identification of SMX transformation products

(TPs) and their evolution over time, carried out by liquid chromatography-mass spectrometry (LC-MS). SMX transformation was conducted through halogenation, dimerization and oxidation pathways, involving mainly RHS. Most of the detected transformation products accumulated over time (up to 360 min of irradiation). These findings bring concerns about the viability of photocatalytic water treatments using $TiO_2$ NPs in saline waters, as RHS could be yielded resulting in the generation and accumulation of halogenated organic byproducts.

## 1. Introduction

In recent years, titanium dioxide as nanoparticles ($TiO_2$ NPs), has been one of the most employed photocatalysts in heterogeneous Advanced Oxidation Processes (AOPs) for water treatment, due to its low cost and toxicity, and also to its high reactivity and chemical stability (Riaz and Park, 2020). One of the advantages of heterogeneous photocatalysis compared with other AOPs is the possibility to use natural light, like sunlight irradiation, as energy source (Martins et al., 2019). Heterogeneous photocatalysis has been proved to efficiently remove a wide range of micropollutants, such as pesticides and pharmaceuticals (Byrne et al., 2018; Mahmoud et al., 2017). This degradation of trace organic compounds is known to occur by the oxidizing activity of reactive oxygen species (ROS), which is characteristic of the photoactivation process of $TiO_2$ in water.

In pure water, the generation mechanism of ROS during $TiO_2$ photoactivation such as hydroxyl ($^{\bullet}OH$) and superoxide ($O_2^{\bullet-}$) radicals, as well as hydrogen peroxide ($H_2O_2$) and singlet oxygen ($^1O_2$) is a well-known process, summarized in reactions 1 to 6 (Fujishima et al., 2008; Nosaka and Nosaka, 2017; Rodríguez et al., 2014). $TiO_2$ is known to have semiconductor properties. Thus, when this material absorbs radiation with enough energy to overcome its band gap, electrons ($e^-$) are excited from the valence band to the conduction band, generating holes ($h^+$)

in the valence band (reaction 1). Then, on one hand, the promoted $e^-$ of the conduction band can be captured by dissolved $O_2$ in its triplet state, promoting the generation of $O_2^{\bullet-}$ (reaction 2) and avoiding the recombination process between $e^-$ and $h^+$. Additionally, at acidic pH conditions, $O_2^{\bullet-}$ may be also present in its protonated form ($HO_2^\bullet$, pKa = 4.8) and lead to further production of $H_2O_2$ and $^\bullet OH$ (reactions 3 and 4). On the other hand, in the photogenerated hole, $^\bullet OH$ is produced by the oxidation of $H_2O$ (reaction 5), whereas $^1O_2$ can be produced by the oxidation of the previously generated $O_2^{\bullet-}$ (reaction 6).

$$TiO_2 + h\nu \longrightarrow e^- + h^+ \quad (1)$$

$$O_2 + e^- \longrightarrow O_2^{\bullet-} \quad (2)$$

$$2HO_2^\bullet \longrightarrow H_2O_2 + O_2 \quad (3)$$

$$HO_2^\bullet + H_2O_2 \longrightarrow H_2O + O_2 + {}^\bullet OH \quad (4)$$

$$H_2O + h^+ \longrightarrow {}^\bullet OH + H^+ \quad (5)$$

$$O_2^{\bullet-} + h^+ \longrightarrow {}^1O_2 \quad (6)$$

On the other hand, photocatalytic treatments with $TiO_2$ are considered as treatment option for micropollutants abatement in saline waters and seawater (D. Camacho-Muñoz, 2020) and also for disinfection (Romero-Martínez et al., 2014; Rubio et al., 2013). However, the photoactivation mechanism of $TiO_2$ in seawater has not been completely established. According to the previous knowledge regarding the $TiO_2$-UV mechanisms in pure water, it could be hypothesized that similar processes involving ROS generation could be also observed in seawater. However, recent studies suggest that the high content in halides ions of seawater may modify the chemistry of the process, this resulting in the generation and subsequent participation of reactive halogen species (RHS). This was indirectly inferred by Hao and co-workers, who observed that $TiO_2$ NPs promoted halogenation of dissolved organic matter (DOM) under sunlight irradiation in seawater (Hao et al., 2018). As known, many halogenated

77 organic compounds may display toxic properties and thus become a risk to the environment
78 and human health (Jiang et al., 2017; Liu and Zhang, 2014). For this reason, understanding the
79 underlying photoactivation mechanisms taking place in photocatalytic treatments of saline
80 waters is essential for a better assessment of the potential risks derived from the release of
81 halogenated transformation products into the environment.
82
83 Sulfamethoxazole (SMX) has been one of the most studied micropollutants in water treatment
84 in a wide variety of advanced oxidation processes. Among others, SMX was used in
85 photocatalytic degradation experiments with $TiO_2$, under solar irradiation and artificial light
86 sources (Borowska et al., 2019; Martins et al., 2019). Consequently, SMX degradation
87 mechanism by photocatalysis in pure water is well known.
88
89 The aim of this work was to investigate the degradation mechanisms taking place when
90 photocatalytic treatment with $TiO_2$ is implemented in saline waters such as seawater. To do so,
91 photocatalytic degradation experiments with SMX were conducted in the presence of $TiO_2$ NPs
92 under controlled irradiation conditions (*i.e.*, simulated sunlight) in a standard seawater matrix.
93 The relative contribution of the different generated reactive species was completed by the
94 application of selective radical scavengers in degradation tests. These experiments, together
95 with a comprehensive identification and monitoring of reaction intermediates formed during
96 SMX degradation, allowed the elucidation of the corresponding reactive halide species
97 generation mechanism and their main reaction pathways.
98
99 **2. Materials and methods**
100 *2.1 Chemicals and reagents*
101 Sulfamethoxazole and *tert*-butanol were purchased from Sigma-Aldrich (Germany). Titanium
102 dioxide (Degussa P25), was acquired from Evonik (Germany). Sodium chloride, magnesium

103 chloride hexahydrate, calcium chloride dihydrate, potassium chloride, sodium hydrogen
104 carbonate, potassium bromide, boric acid, sodium hydroxide, sodium azide and acetonitrile
105 were supplied by Panreac (Spain). Sodium sulfate and *p*-benzoquinone were purchased from
106 Probus (Spain) and Merck Schuchardt OHG (Germany), respectively. Pure nitrogen gas
107 (99.995%) was acquired from Abelló Linde (Spain).
108
109 *2.2 Photocatalytic experiments*
110 Degradation experiments were performed in simulated seawater (SW) and in deionized water
111 (DW), for comparison purposes. Simulated seawater was prepared according to the ASTM
112 D1141-98 standard (ASTM international, 2013). The chemical composition of SW is detailed in
113 Table S1 of the Supplementary Information. Its pH was adjusted to 8.2 by the addition of
114 NaOH. For DW, unless otherwise specified, the pH of the solution (pH = 6) was not modified.
115 $TiO_2$ NPs used in this work (Degussa P25) have a content of 80% of anatase and 20% of rutile,
116 and a BET surface between 35 and 65 $m^2$ $g^{-1}$. The band gap is 3.2 eV and particles have a mean
117 diameter of 21 nm.
118 The concentration of SMX and $TiO_2$ NPs used for degradation experiments was 1 mg $L^{-1}$ and
119 100 mg $L^{-1}$, respectively. For the transformation products characterization study, the
120 concentrations increased to 10 mg $L^{-1}$ of SMX and 1000 mg $L^{-1}$ of $TiO_2$ NPs, for a better
121 identification of the formed byproducts.
122 Irradiation experiments were conducted as follows: aqueous solutions were placed into a 1L
123 jacketed reservoir tank with continuous magnetic stirring. After that, these were continuously
124 pumped with a peristaltic pump, into a Duran glass tubular photoreactor (diameter and length
125 of 2 and 24.5 cm, respectively), placed inside the solar simulation chamber Xenoterm-1500RF,
126 CCI (Spain), and then recirculated back to the reservoir tank. The solar simulation chamber was
127 equipped with a Xenon lamp (1.5 kW) emulating the solar spectrum. Radiation with
128 wavelengths below 290 nm was cut-off by the Duran glass of the photoreactor. An *o*-

129 nitrobenzaldehyde actinometry was employed to establish the photonic flow in the
130 wavelength range of 290-400 nm, being this 0.66 µEinstein $s^{-1}$ (Bustos et al., 2019). A
131 thermostatic bath was used to keep the tank temperature at 20 $^{o}$C during the irradiation
132 process. The irradiation time was 120 min for all the experiments, except for the intermediates
133 study where it was extended up to 360 min. In the first case, aliquots of 10 mL were extracted
134 from the reservoir tank at different irradiation times and then filtered with 0.45 µm PVDF
135 filters. For degradation experiments, data were obtained, at least, in duplicates. The values
136 plotted showed deviations below 5%. In the intermediates study, due the observed
137 interference of the salts in the mass spectrometry analysis and for a suitable detection of the
138 intermediates generated, a solid phase extraction (SPE) treatment was employed. Aliquots of
139 40 mL were extracted from the reservoir tank at the irradiation times of 0, 30, 120, 240 and
140 360 min, and filtered with 0.45 µm PVDF filters. After that, SPE cartridges Oasis HLB 20 cc $g^{-1}$
141 acquired from Waters Corporation (USA), were loaded with the corresponding aliquots, then
142 washed with 40 mL of deionized water. Extraction of organic components (*i.e.*, SMX and
143 reaction intermediates) was finally achieved with 8 mL of acetonitrile. This way, salts were
144 removed and the organic components in original samples were concentrated 3 times.
145
146 *2.3 Analytical methods*
147 The SMX degradation in irradiation experiments was evaluated by an Infinity 1260 HPLC
148 provided by Agilent Technologies (USA). The employed column was a Mediterranea Sea 18
149 (250 mm x 4.6 mm and 5 µm particle size) supplied by Teknokroma (Spain). The mobile phases
150 used consisted of volumetric mixtures containing 60% of acetonitrile and 40% of ultrapure
151 water adjusted with orthophosphoric acid at pH 3. The flux employed was 1.1 mL $min^{-1}$ and the
152 UV detector was set at 270 nm. The injection volume was set to 50 µL and the column
153 temperature was set to 30 $^{o}$C.
154

155 The intermediates identification was performed by liquid chromatography-mass spectrometry
156 (LC-MS) with an Agilent 1100 HPLC coupled to G1969A LC/MSD-TOF mass spectrometer. All
157 intermediates were detected in negative electrospray ionization mode (ESI (-)) with a
158 fragmentor voltage of 150 V and collected in a scan range of 50-1100 m/z. Data in extracted
159 ion chromatograms (EIC) were employed for the monitoring of the intermediates in the
160 different samples. The chromatographic separation was performed with the same column
161 used in the Infinity 1260 HPLC analyses and a volumetric mixture containing 40% of milli Q
162 water and 60% of acetonitrile as mobile phase. As for the SMX degradation experiments, in the
163 byproducts study the column temperature was also set to 30 $^{o}$C but in this case the injection
164 volume was set to 2 μL.
165
166 **3. Results and discussion**
167 *3.1 Evaluation of photoactivation of $TiO_2$ NPs in seawater, under simulated sunlight irradiation*
168 Photoactivation of $TiO_2$ NPs under simulated sunlight was studied assessing the degradation of
169 SMX as a model organic compound. Initially, a control experiment was conducted in order to
170 test SMX adsorption with $TiO_2$ NPs under dark conditions in the seawater matrix. Photolysis of
171 SMX by simulated sunlight irradiation was also assessed. After 120 min, SMX degradation was
172 1% and 3%, respectively, suggesting the lack of SMX adsorption and the negligible photolysis
173 contribution to the SMX degradation.
174
175 Photocatalytic degradation of 1 mg $L^{-1}$ SMX with $TiO_2$ in the SW matrix was evaluated by the
176 addition of different concentrations of $TiO_2$ (10, 100 and 1000 mg $L^{-1}$). Although concentrations
177 of $TiO_2$ NPs and micropollutants in the aquatic environment are typically lower (*i.e.*, in the
178 range from ng to μg $L^{-1}$), these experimental conditions were selected to magnify the process
179 so that this could be studied in a reasonable lapse of time. The final degradation after 120 min
180 of irradiation and the corresponding pseudo-first order rate constants obtained were 14%

181 (0.001 $min^{-1}$), 91% (0.020 $min^{-1}$) and 100% (0.079 $min^{-1}$), respectively, which demonstrate the
182 photodegradation activity of the process in seawater. According to the results, a concentration
183 of 100 mg $L^{-1}$ of $TiO_2$ was selected for performing degradation experiments. Results in SW were
184 compared with DW using 100 mg $L^{-1}$ of $TiO_2$. After 120 min of irradiation, a complete SMX
185 degradation was obtained, with a pseudo-first order rate constant of 0.041 $min^{-1}$, (Fig. 1), that
186 is two times faster than that in SW.

187

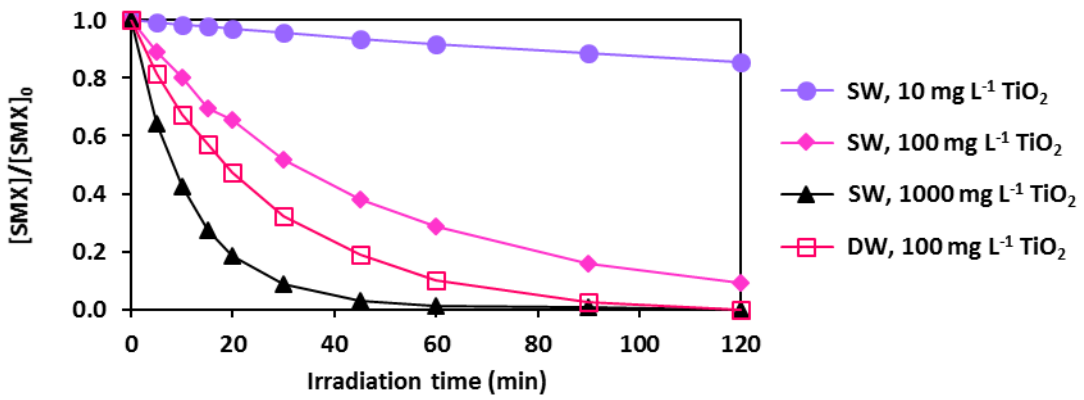


188

189 **Figure 1.** Degradation of SMX using different concentration of $TiO_2$ in SW compared with 100
190 mg $L^{-1}$ in DW.

191

192 *3.2 Identification of reactive species generated from photoactivation of $TiO_2$ NPs in seawater*

193 The study of the contribution of the different reactive oxygen species (ROS), such as $^{\bullet}OH$, $O_2^{\bullet-}$,
194 and other possible radical and oxidizing agents formed in the photocatalytic process was
195 carried out by the addition of selected radical scavengers. For the determination of the $^{\bullet}OH$
196 contribution in the bulk solution, photocatalytic experiments were performed with the
197 presence of *tert*-butanol (TBA), which has a reaction rate constant with $^{\bullet}OH$ of 6.0 x $10^8$ $M^{-1}$ $s^{-1}$
198 (Buxton et al., 1988). Dissolved oxygen promotes the photocatalytic reaction by trapping the
199 excited electron of the $TiO_2$ conduction band, generating superoxide radical ($O_2^{\bullet-}$) and
200 avoiding the recombination process. 1,4-benzoquinone (BQ) has been used by different
201 researchers as scavenger of $O_2^{\bullet-}$(Jedsukontorn et al., 2018; Xiao et al., 2016; Zhang et al.,

202 2017) because of its high reactivity with this species (rate constant value of 9.8 x $10^8$ $M^{-1}$ $s^{-1}$
203 (Bielski et al., 1985)). However, BQ has also a high reactivity with $^{\bullet}OH$ (6,6 x $10^9$ $M^{-1}$ $s^{-1}$ (Buxton
204 et al., 1988)). Thus, if $^{\bullet}OH$ is expected to be involved in the degradation process, the whole
205 interaction with BQ should be considered (Rodríguez et al., 2014). Moreover, by removing
206 dissolved oxygen by bubbling the solution with $N_2$, the overall contribution of dissolved oxygen
207 on the promotion of radical species can be assessed (García-Fernández et al., 2015; Rodríguez
208 et al., 2014). Another possible ROS generated in the photocatalytic process is singlet oxygen
209 ($^1O_2$), which mainly comes from the oxidation of $O_2^{\bullet-}$ by the hole ($h^+$). To determine the $^1O_2$
210 participation on the SMX degradation, many works in literature report the use of sodium azide
211 ($NaN_3$) as scavenger of this oxidizing agent (Fotiou et al., 2016; Tiwari et al., 2019; Xiao et al.,
212 2016) because of the high reactivity between both species (rate constant of 2.1 x $10^9$ $M^{-1}$ $s^{-1}$)
213 (Catalán et al., 2004). However, $N_3^-$ has also a high rate constant with $^{\bullet}OH$ (1.2 x $10^{10}$ $M^{-1}$ $s^{-1}$),
214 generating $^{\bullet}N_3$ , also a reactive radical (Buxton et al., 1988). Thus, a double scavenging effect of
215 $N_3^-$ should be considered if $^{\bullet}OH$ is expected to be generated in the photocatalytic process
216 (Rodríguez et al., 2014). The $h^+$ participation in the SMX degradation can be evaluated by the
217 addition of formic acid (FA), which is able to suppress all the $h^+$ processes (Doudrick et al.,
218 2013). These include: 1) the direct oxidation of SMX by $h^+$, 2) the possible generation of $^1O_2$
219 from $O_2^{\bullet-}$, 3) the generation of $^{\bullet}OH$ through the oxidation of $H_2O$ and 4) the production of
220 other oxidant species (Cavalcante et al., 2016; Ribao et al., 2019; Zheng et al., 2010).
221 Additionally, if $^{\bullet}OH$ is generated in the system through other pathways, FA is also able to
222 scavenge this oxidant because of the high rate constant value of their corresponding reaction
223 (3.2 x $10^9$ $M^{-1}$ $s^{-1}$ as formate ion at neutral pH (Buxton et al., 1988)).
224
225 Results of the addition of the different scavengers (3 mM of TBA, 3 mM of $NaN_3$, 11 and 560
226 mM of FA as well as 0.075 and 0.25 mM of BQ), with 100 mg $L^{-1}$ of $TiO_2$ and 1 mg $L^{-1}$ of SMX, in
227 SW and also in DW, are shown in Fig. 2A and 2B, respectively. Unless otherwise specified, the

concentration of scavenger employed in each test was selected to represent at least 95% of the total scavenging effect exerted over the oxidant under evaluation.

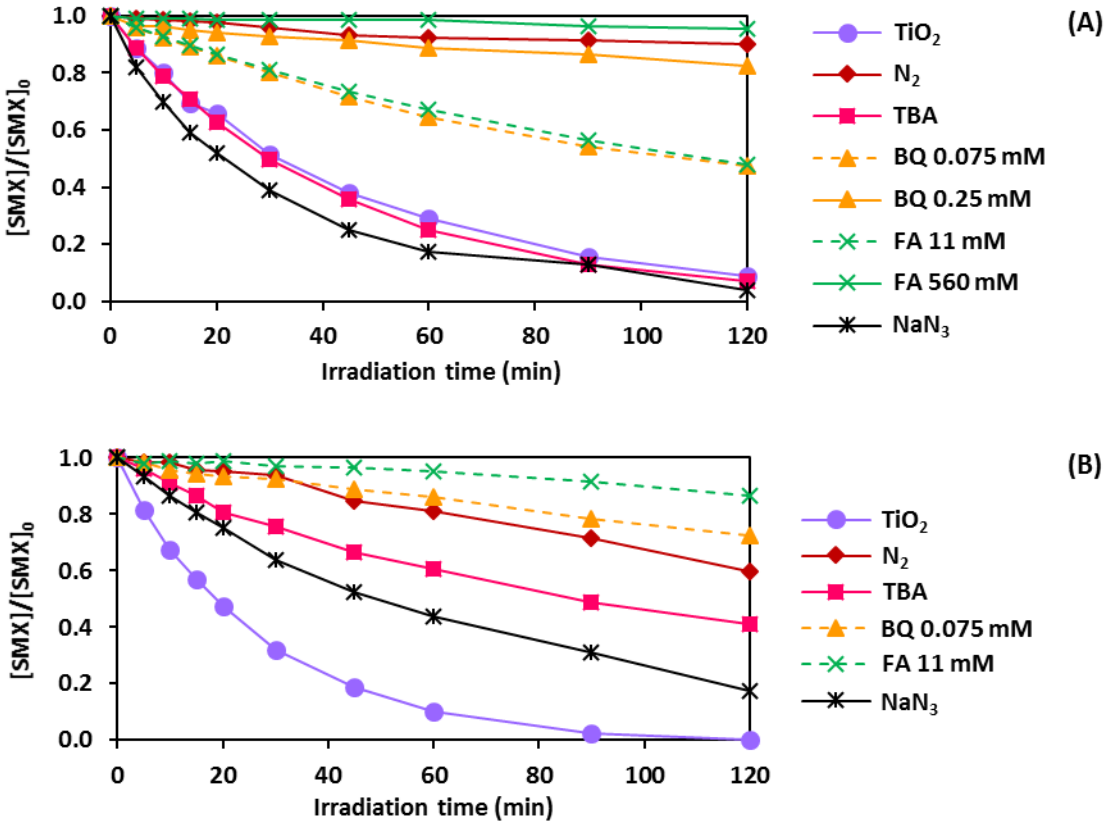


**Figure 2.** Effect in the SMX degradation by the addition of different scavengers in A) SW and B) DW.

The most significant difference between activation of $TiO_2$ NPs in seawater and deionized water was for the tests performed with TBA. In SW, no inhibition of SMX degradation was observed, indicating that the degradation process is not mediated by $^{\bullet}OH$ in the bulk solution. This result confirms that the mechanism of the photocatalytic degradation process in SW is different from DW, where circa 60% of the SMX degradation occurred by the $^{\bullet}OH$ in the bulk solution, as it can be seen in Fig. 2B.

243 Experiments with FA in SW also generated significant findings. Tests were performed at two
244 different concentrations, 11 mM and 560 mM. The employment of 11 mM is based on other
245 studies that used similar concentration to block the $h^+$ pathway in DW (Zheng et al., 2010). On
246 the other hand, the experiment with 560 mM of FA was conducted to reach the same
247 concentration of chlorine anions ($Cl^-$) in SW, with the aim of overcoming potential competition
248 of this species in the FA adsorption on the $TiO_2$ surface. Results for 11 mM and 560 mM of FA
249 showed that, after 120 min, the SMX degradation was inhibited from 91% to 52% and from
250 91% to 5%, respectively. Thus, 560 mM of FA were able to avoid the $h^+$ pathway, suggesting
251 that, in SW, halide species may directly participate in the redox mechanism that takes place in
252 the hole. In the case of experiments in DW, only the 11 mM FA test was carried out. In this
253 assay in particular, the pH of the solution was adjusted to 6 with the addition of NaOH in order
254 to keep the same pH of the other experiments in DW. Results showed an almost complete
255 inhibition of the SMX degradation, from 100% to 14%, which was also attributed to the
256 impediment of the $h^+$ pathway avoiding the generation of the $^{\bullet}OH$.
257
258 Other tests with selected scavengers also provided complementary information about $TiO_2$
259 NPs photoactivation in seawater. The removal of dissolved oxygen from the solution, by
260 bubbling it with $N_2$, led to almost total inhibition of the SMX degradation, resulting just 10%
261 removal after 120 min of irradiation. This result remarks the importance of the presence of
262 dissolved oxygen to inhibit the recombination of e-/h+ and thus allow the performance of the
263 photocatalytic reactions. In the case of DW, the inhibition was weaker compared with SW,
264 allowing 40% removal in 120 min.
265
266 The experiment performed with a BQ concentration of 0.075 mM resulted in a SMX
267 degradation inhibited from 91% to 52%. By increasing the BQ concentration to 0.25 mM, SMX
268 degradation inhibition was even more significant, down to 18%. These differences in the BQ

269 inhibition capacity suggest that, in addition to the reaction of BQ with $O_2^{\bullet-}$, this reagent may
270 undergo reactions with other oxidant species, which in fact would be the main responsible for
271 the observed SMX degradation. In similar experiments conducted with DW and 0.075 mM of
272 BQ, SMX degradation was inhibited from 100% to 27%. This strong inhibition can be explained
273 by the presence of $^{\bullet}OH$ in the bulk solution, as BQ may react with both $O_2^{\bullet-}$ and $^{\bullet}OH$, resulting
274 this in a double inhibition effect over the SMX degradation.
275
276 Finally, $NaN_3$ test in SW revealed no participation of $^1O_2$ in the SMX degradation. In DW, the
277 SMX degradation was inhibited from 100% to 82% in 120 min. However, the reactivity of $^-N_3$
278 with $^{\bullet}OH$ generate $^{\bullet}N_3$, which may as well behave as an oxidant (An et al., 2010; Bancirova,
279 2011) and thus participate on the SMX degradation in DW.
280
281 According to the obtained results, when $TiO_2$ NPs are present in seawater, the oxidizing species
282 produced in the redox process at the hole may involve the participation of halide ions that are
283 found at high concentration in this water matrix (560 mM and 0.8 mM for $Cl^-$ and $Br^-$,
284 respectively). Therefore, the oxidative role of $^{\bullet}OH$, which is the main responsible of the SMX
285 degradation in deionized water, may be replaced by reactive halogen species in saline waters.
286 Different authors previously studied the reactivity of halide ions with the $TiO_2$ photogenerated
287 hole to promote the formation of free halogen radicals (reactions 7 and 8), which may later
288 generate other reactive halogen species (RHS) (Boutiti et al., 2017; Daimon et al., 2008). RHS
289 comprise radical and non-radical species, such as $X^{\bullet}$, $X_2^{\bullet-}$, $HOX^{\bullet-}$, HOX, $^-OX$ and $X_2$, where X
290 corresponds to Cl or Br, as presented in reactions 7 to 41 (Grebel et al., 2009). These species
291 are less reactive but more selective oxidants than $^{\bullet}OH$, being mainly involved in reactions with
292 compounds containing electron-rich functional groups (Grebel et al., 2009).
293

$$Cl^- + h^+ \longrightarrow Cl^\bullet \quad (7)$$

$$Br^- + h^+ \longrightarrow Br^\bullet \quad (8)$$

$$Cl^\bullet + {}^-OH \leftrightarrow HOCl^{\bullet-} \leftrightarrow Cl^- + {}^\bullet OH \quad (9)$$

$$Br^\bullet + {}^-OH \leftrightarrow HOBr^{\bullet-} \leftrightarrow Br^- + {}^\bullet OH \quad (10)$$

$$Cl^\bullet + Cl^\bullet \longrightarrow Cl_2 \quad (11)$$

$$Br^\bullet + Br^\bullet \longrightarrow Br_2 \quad (12)$$

$$Cl^\bullet + Br^- \longrightarrow BrCl^{\bullet-} \quad (13)$$

$$Br^\bullet + Cl^- \longrightarrow BrCl^{\bullet-} \quad (14)$$

$$Cl^\bullet + Cl^- \longrightarrow Cl_2^{\bullet-} \quad (15)$$

$$Br^\bullet + Br^- \longrightarrow Br_2^{\bullet-} \quad (16)$$

$$Cl_2^{\bullet-} + O_2^{\bullet-} \longrightarrow 2Cl^- + O_2 \quad (17)$$

$$Br_2^{\bullet-} + O_2^{\bullet-} \longrightarrow 2Br^- + O_2 \quad (18)$$

$$Cl_2^{\bullet-} + Cl_2^{\bullet-} \longrightarrow Cl_2 + 2Cl^- \quad (19)$$

$$Br_2^{\bullet-} + Br_2^{\bullet-} \longrightarrow Br_2 + 2Br^- \quad (20)$$

$$Cl_2 + O_2^{\bullet-} \longrightarrow Cl_2^{\bullet-} + O_2 \quad (21)$$

$$Br_2 + O_2^{\bullet-} \longrightarrow Br_2^{\bullet-} + O_2 \quad (22)$$

$$Cl_2 + H_2O \longrightarrow HOCl + Cl^- + H^+ \quad (23)$$

$$Br_2 + H_2O \longrightarrow HOBr + Br^- + H^+ \quad (24)$$

$$HOCl \leftrightarrow {}^-OCl + H^+ \quad (25)$$

$$HOCl \leftrightarrow {}^-OBr + H^+ \quad (26)$$

$$HOCl^{\bullet-} + Cl^- \longrightarrow Cl_2^{\bullet-} + {}^-OH \quad (27)$$

$$HOBr^{\bullet-} + Br^- \longrightarrow Br_2^{\bullet-} + {}^-OH \quad (28)$$

$$HOCl^{\bullet-} + Br^- \longrightarrow BrCl^{\bullet-} + {}^-OH \quad (29)$$

$$HOBr^{\bullet-} + Cl^- \longrightarrow BrCl^{\bullet-} + {}^-OH \quad (30)$$

$$Cl^\bullet + Br^- \longrightarrow BrCl^{\bullet-} \quad (31)$$

$$Br^\bullet + Cl^- \longrightarrow BrCl^{\bullet-} \quad (32)$$

$$Cl_2^{\bullet-} + Br^- \longrightarrow BrCl^{\bullet-} + Cl^- \quad (33)$$

$$Br_2^{\bullet-} + Cl^- \longrightarrow BrCl^{\bullet-} + Br^- \quad (34)$$

$$BrCl^{\bullet-} + Cl_2^{\bullet-} \longrightarrow 2Cl^- + BrCl \quad (35)$$

$$BrCl^{\bullet-} + Br_2^{\bullet-} \longrightarrow Br_2 + Br^- + Cl^- \quad (36)$$

$$BrCl^{\bullet-} + Cl^- \longrightarrow Cl_2^{\bullet-} + Br^- \quad (36)$$

$$BrCl^{\bullet-} + Br^- \longrightarrow Br_2^{\bullet-} + Cl^- \quad (37)$$

$$BrCl^{\bullet-} + O_2^{\bullet-} \longrightarrow Br^- + Cl^- + O_2 \quad (38)$$

$$BrCl^- + O_2^{\bullet-} \longrightarrow BrCl^{\bullet-} + O_2 \quad (39)$$

$$Br_2^{\bullet-} + Cl_2^{\bullet-} \longrightarrow Br_2 + 2Cl^- \quad (40)$$

$$BrCl^{\bullet-} + BrCl^{\bullet-} \longrightarrow BrCl + Br^- + Cl^- \quad (41)$$

RHS could also result from the reaction of $^\bullet OH$, in case of its primary generation in the $h^+$, with halides (reaction 9 and 10). However, because of the lack of inhibition of SMX degradation in the TBA experiment, this pathway is unlikely to occur. This observation, together with the complete inhibition of the $h^+$ pathway by FA at high concentration (similar to $Cl^-$), points out that the direct oxidation of halides in the photoactivated holes in saline matrices are the main promoters of RHS. Between halides, $Br^-$ is expected to be more reactive with the hole than $Cl^-$

301 because of its lower reduction potential (($E(Cl^{\bullet}/Cl^{-}) = 2.5\ V_{NHE} > ((E(Br^{\bullet}/Br^{-}) = 2.0\ V_{NHE})$) (Zhang
302 and Parker, 2018).
303 At the seawater pH (8.2), the equilibrium between $Cl^{\bullet}$ and $^{\bullet}OH$ (reaction 9) is displaced to the
304 $^{\bullet}OH$ formation (von Sonntag and von Gunten, 2012). Consequently, TBA experiments should
305 also have shown some inhibition of SMX degradation by $^{\bullet}OH$ scavenging, which was not the
306 observed situation. However, it must be taken into account that the equilibrium between $Br^{\bullet}$
307 and $^{\bullet}OH$ is displaced to the production of $BrOH^{\bullet-}$ under the same conditions (reaction 10),
308 subsequently yielding $BrCl^{\bullet-}$ (reaction 30) (Zhang and Parker, 2018). Hence, the lack of
309 inhibition of SMX degradation in the TBA experiment may be justified by the scavenging effect
310 of $Br^{-}$ towards $^{\bullet}OH$ generated through reaction 9 that would compete with TBA, minimizing its
311 scavenging effect. This is also in accordance with the higher kinetic constant of $Br^{-}$ with $^{\bullet}OH$
312 ($1.1 \times 10^{10}\ M^{-1}\ s^{-1}$) compared with the TBA with $^{\bullet}OH$ ($6.0 \times 10^{8}\ M^{-1}\ s^{-1}$).
313 Additionally, Daimon and co-workers, observed a competition between halogen radicals ($Cl^{\bullet}$
314 and $Br^{\bullet}$) and dissolved $O_2$ for the photoexcited electron of the conduction band (Daimon et al.,
315 2008). This fact was observed with the inhibition of SMX degradation when dissolved $O_2$ was
316 removed from the solution (Fig. 2A), suggesting that halogen radicals recovered the electron
317 previously donated to $h^{+}$, inactivating RHS production. This fact supports the suggested
318 primary pathway for the RHS generation by the direct reactivity of halides with the
319 photogenerated hole. Thus, once RHS are produced in the hole, more RHS could be formed
320 through the reactivity of $O_2^{\bullet-}$ with other RHS (reactions 21, 22 and 39).
321 In view of all these considerations, $TiO_2$ photoactivation mechanism is proposed and presented
322 in Fig. 3.

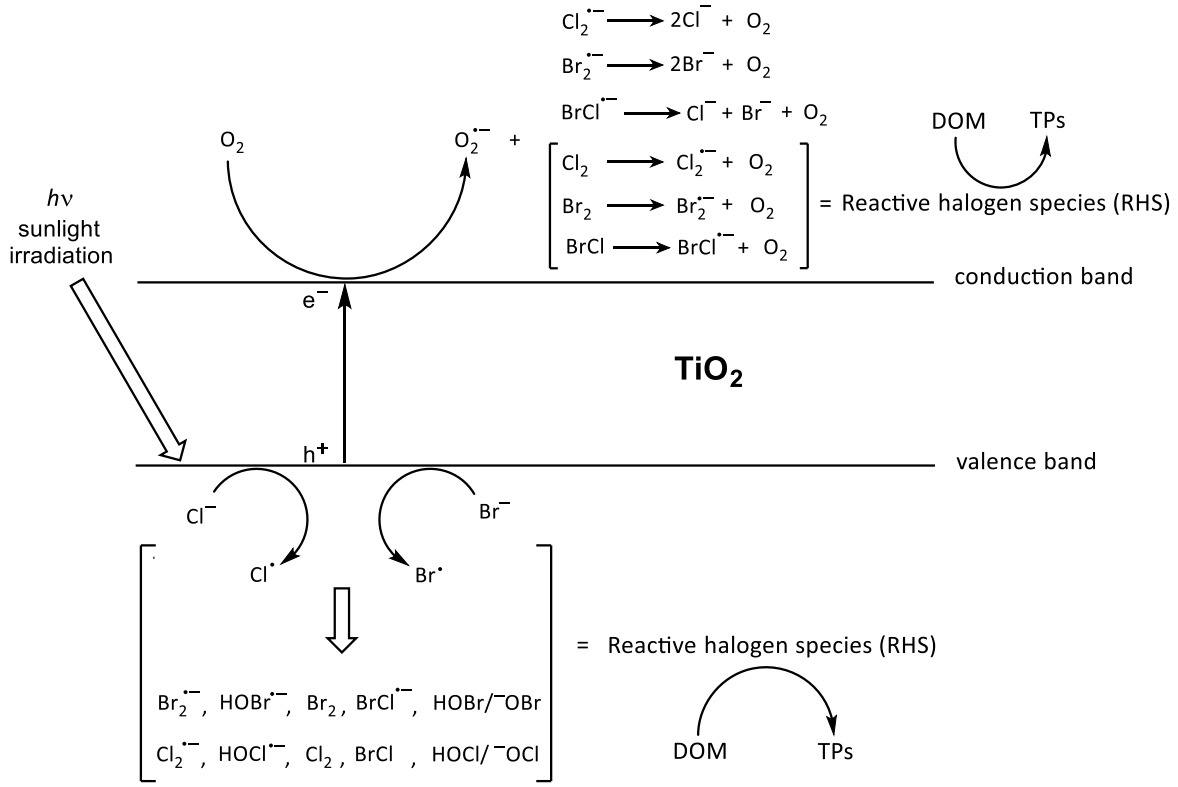


**Figure 3.** Proposed $TiO_2$ photoactivation mechanism in SW for the generation of RHS.

In short, results obtained confirm the different reactive species whose generation is photoinduced by solar radiation and nanosized $TiO_2$, when this pollutant is present in different environmental water matrices. The mechanisms taking place in the aqueous environment are expected to lie between a process governed by ROS generation, in the case of low salinity waters, to another characterized and controlled by RHS production in the case of seawater, as proposed in Fig. 3. Between these two mechanisms, increasing contribution of RHS to derived reactions such as those concerning transformation of organic compounds is expected to occur as salinity of the aqueous medium increases.

*3.3 Generation and evolution of sulfamethoxazole transformation products over seawater photocatalytic treatment*

338 In order to corroborate the observed contribution of RHS in the photocatalytic degradation of
339 SMX in SW, HPLC-MS analyses were performed in samples withdrawn at different irradiation
340 times to identify the main intermediate products generated. To do so, SMX and $TiO_2$
341 concentrations employed were increased to 10 mg $L^{-1}$ and 1000 mg $L^{-1}$, respectively, for a
342 better detection of transformation products.
343
344 A total of 17 TPs were distinguished during the SMX degradation in SW, as shown in Table 1.
345 The relative evolution of the formed intermediates during the photocatalytic process in SW
346 was followed through min-max normalization of the areas obtained by the extracted ion
347 chromatogram. These data are represented in Fig. 4. Based on identified intermediate
348 products and their corresponding evolutions, a mechanism for SMX transformation in the
349 sunlight-$TiO_2$ process in SW was proposed and presented in Fig. 5.
350
351
352 **Table 1.** SMX and TPs identified in HPLC-MS analysis with ESI (-).

| Molecular structure, molar mass (g/mol) and designation | Molecular Formula | LC-MS $[M–H]^–$ (m/z) |
|---|---|---|
| 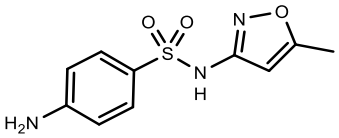 **SMX** M = 253.28 | $C_{10}H_{11}N_3O_3S$ | 252.04 |
| 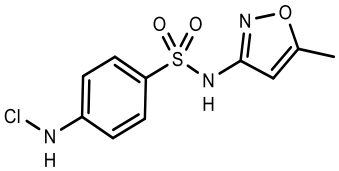 **SMX-Cl** M = 287.72 | $C_{10}H_{10}ClN_3O_3S$ | 286.01-288.01 |
| 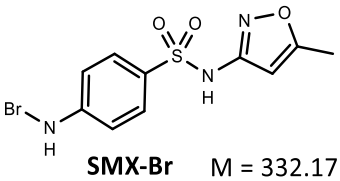 **SMX-Br** M = 332.17 | $C_{10}H_{10}BrN_3O_3S$ | 329.96-331.96 |

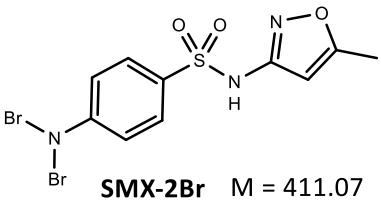

**SMX-2Br** M = 411.07

$C_{10}H_9Br_2N_3O_3S$ 407.87-409.86-411.86

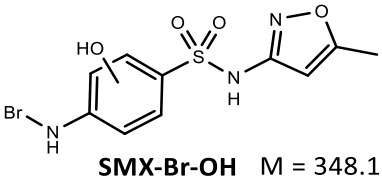

**SMX-Br-OH** M = 348.17

$C_{10}H_{10}BrN_3O_4S$ 345.95-347.95

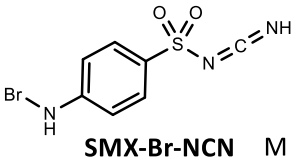

**SMX-Br-NCN** M = 276.11

$C_7H_6BrN_3O_2S$ 273.93-275.93

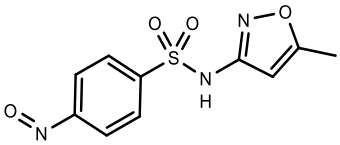

**SMX-NO** M = 267.26

$C_{10}H_9N_3O_4S$ 266.03

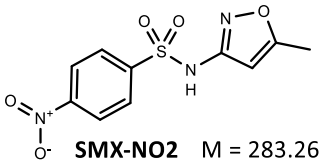

**SMX-NO2** M = 283.26

$C_{10}H_9N_3O_5S$ 282.02

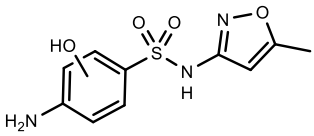

**SMX-OH** M = 269.28

$C_{10}H_{11}N_3O_4S$ 268.04

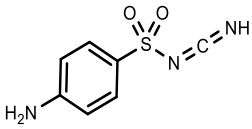

**SMX-NCN** M = 197.21

$C_7H_7N_3O_2S$ 196.02

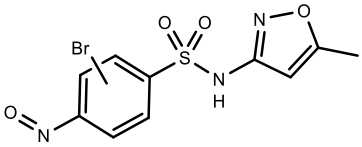

**SMX-Br-NO** M = 346.16

$C_{10}H_8BrN_3O_4S$ 343.95-345.95

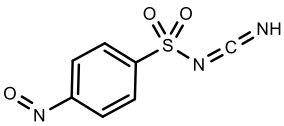

**SMX-NO-NCN** M = 211.20

$C_7H_5N_3O_3S$ 210.00

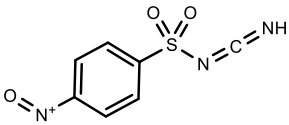

**SMX-NO2-NCN** M = 227.20

$C_7H_5N_3O_4S$ 225.99

| | | |
|---|---|---|
| 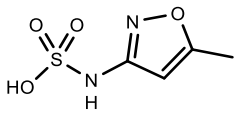 **SMX-SO3H** M = 178.17 | $C_4H_6N_2O_4S$ | 177.00 |
| 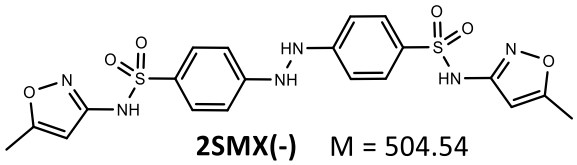 **2SMX(-)** M = 504.54 | $C_{20}H_{20}N_6O_6S_2$ | 503.08 |
| 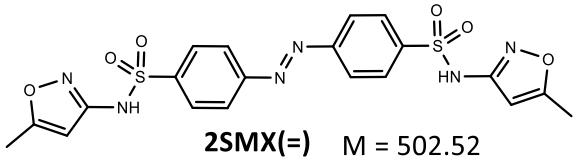 **2SMX(=)** M = 502.52 | $C_{20}H_{18}N_6O_6S_2$ | 501.07 |
| 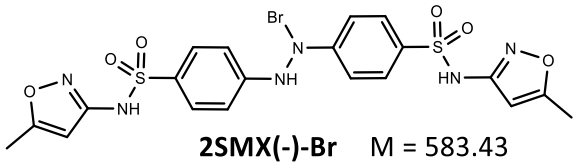 **2SMX(-)-Br** M = 583.43 | $C_{20}H_{19}BrN_6O_6S_2$ | 580.99-582.99 |
| 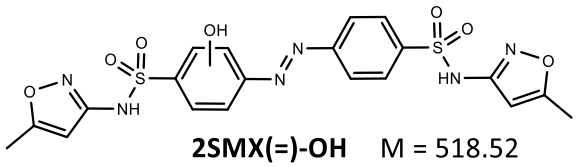 **2SMX(=)-OH** M = 518.52 | $C_{20}H_{18}N_6O_7S_2$ | 517.06 |

According to the MS data, SMX transformation occurred through three primary pathways, halogenation, oxidation and dimerization, mainly driven by RHS.

The halogenation and dimerization pathways (Fig. 5, red arrows and blue arrows, respectively) may initiate through H-abstraction of the phenylamine nitrogen by halogen radical species, such as $Cl^{\bullet}$, $Br^{\bullet}$, $HOCl^{\bullet-}$, $HOBr^{\bullet-}$, $BrCl^{\bullet-}$, $Cl_2^{\bullet-}$ and $Br_2^{\bullet-}$, leading to the formation of the $SMX^{\bullet}$ molecule. Further halogen radical species addition to the generated $SMX^{\bullet}$ molecule would end in the formation of primary halogenated TPs. At the same time, two $SMX^{\bullet}$ molecules could interact yielding SMX dimerization. The individuality of the proposed halogenation and dimerization mechanisms is justified in view of the simultaneous formation of their primary TPs (SMX-Cl and SMX-Br) and (2SMX(-)), that reached their maximum concentrations at 120 min of irradiation (see Fig. 4A and 4C).

Five halogenated TPs were detected (Fig. 5, red arrows). The ion fragment at 233.92-235.92 m/z for $(M-H)^-$ (Fig. S1 of Supplementary Information) containing the Br atom in its structure suggests that this addition took place in the phenylamine moiety, most probably at the nitrogen position (Dodd and Huang, 2004; Gao et al., 2014). From the SMX-Br intermediate, three secondary TPs were generated (SMX-2Br, SMX-Br-OH and SMX-Br-NCN). The second bromination to form SMX-2Br possibly took place again in the nitrogen atom of the phenylamine moiety. The observed hydroxylation to generate the SMX-Br-OH intermediate could probably occur in the phenyl ring. Finally, the detected SMX-Br-NCN intermediate may result from the fragmentation of the isoxazole ring. This opening ring mechanism is also reported in literature (Cai and Hu, 2017; Yuan et al., 2019), through a first hydroxylation of the ring followed by its fragmentation.

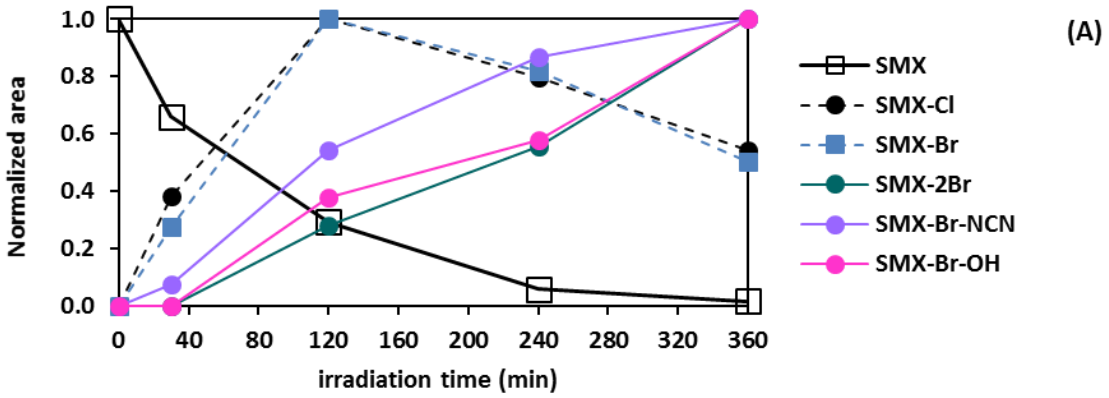


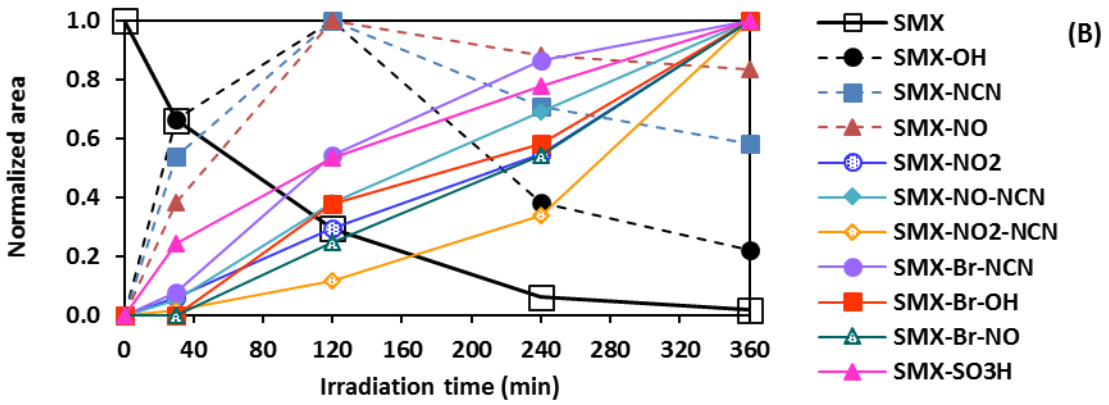

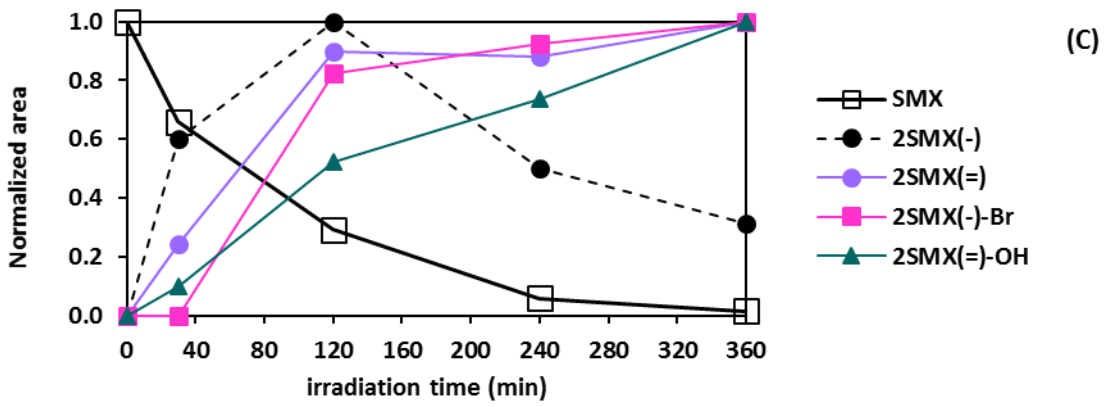


**Figure 4.** Normalized area of the TPs and SMX over the time by the EIC of the mass spectrometer for A) halogenation, B) oxidation and C) dimerization pathways.

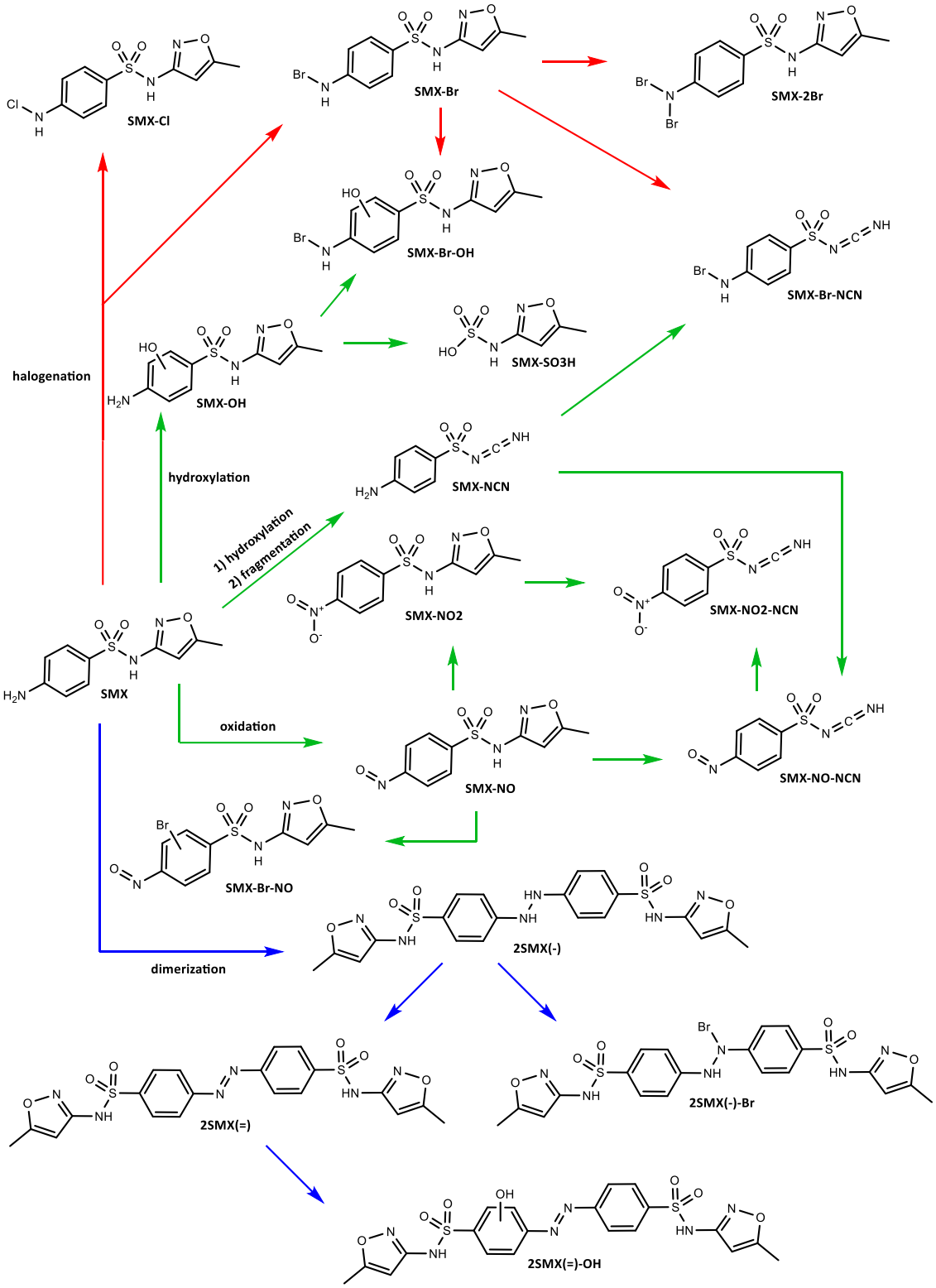


**Figure 5.** SMX intermediates formation mechanism. Red, green and blue arrows refer to the degradation process initiated by halogenation, oxidation and dimerization pathways, respectively.

390 The dimerization pathway (Fig. 5, blue arrows) generated 4 identified TPs. From the primary
391 dimer 2SMX(-), three secondary TPs were identified (2SMX(=), SMX(-)-Br and SMX(=)-OH). The
392 2SMX(-)-Br generation might occur by a bromination of one of the nitrogen atoms of the
393 2SMX(-) hydrazine group. The 2SMX(=) dimeric intermediate is expected to come from a
394 second H-abstraction in the nitrogen atoms of the 2SMX(-) hydrazine group, giving rise to the
395 formation of the azo functional group. Subsequently, the hydroxylation of one of the phenyl
396 groups in the 2SMX(=) TP might lead to the formation of 2SMX(=)-OH.
397
398 Oxidation pathway exhibits different mechanisms and TPs. Despite the TBA scavenger test
399 showed no significant participation of the $^{\bullet}OH$ in the SMX degradation, hydroxylation of the
400 SMX molecule occurred in its degradation process. Among other possibilities, the equilibrium
401 of the reaction 9 and 10 involving $HOCl^{\bullet-}$ and $HOBr^{\bullet-}$ could balance to some $^{\bullet}OH$ production.
402 Other possibility would be the direct hydroxylation performed by some of the RHS as $HOCl^{\bullet-}$,
403 $HOBr^{\bullet-}$, $HOCl/^{-}OCl$ and $HOBr/^{-}OBr$ or even by some secondary reaction involving the $O_2^{\bullet-}$. In
404 any case, 10 oxidized TPs were detected (Fig. 5, green arrows). The primary intermediate SMX-
405 NO may result from the oxidation of the phenylamine group of the SMX molecule to nitroso
406 benzene moiety, which may be conducted by $HOCl/^{-}OCl$ and $HOBr/^{-}OBr$ as suggested in
407 previous studies (Gao et al., 2014). The oxidation of the phenylamine amine group is
408 supported by the fragment ion detected of 169.99 m/z for $(M-H)^{-}$ (Fig. S2 of the
409 Supplementary Information).
410 Formation of the primary intermediate SMX-OH may be apparently performed through
411 hydroxylation of the phenylamine moiety, was corroborated through the identification of the
412 ion fragment of 172.01 m/z for $(M-H)^{-}$ (Fig. S3 of the Supplementary Information). The OH
413 addition probably occurred in the phenyl group, as other authors concluded in previous studies
414 (Dodd and Huang, 2004; Gao et al., 2014; Yuan et al., 2019). Additionally, and even though it
415 was not a primary TP, SMX-NCN was rapidly generated and reached the maximum

416 concentration after 120 min of irradiation (see Fig. 4B). The hydroxylation and fragmentation
417 of the isoxazole ring could thus have been part of the SMX-NCN generation.
418 According to Figure 5, four secondary TPs generated from intermediate SMX-NO were
419 identified (SMX-NO2, SMX-Br-NO, SMX-NO-NCN and SMX-NO2-NCN). Formation of the species
420 SMX-NO2 might be attributed to the oxidation of the nitrosobenzene to nitrobenzene moiety,
421 which was in fact corroborated by the detected ion fragment of 185.99 m/z for $(M-H)^-$ (Fig. S4
422 of the Supplementary Information). Bromination of the nitrobenzene ring could generate SMX-
423 Br-NO TP, and the subsequent hydroxylation and fragmentation of the isoxazole ring might
424 have generated the SMX-NO-NCN TP. Both SMX-NO2 and SMX-NO-NCN are precursors of the
425 intermediate SMX-NO2-NCN, respectively by their hydroxylation/fragmentation and oxidation.
426 From the primary intermediate SMX-OH, two main secondary TPs were identified (SMX-Br-OH
427 and SMX-SO3H). The intermediate SMX-Br-OH was formed from the bromination of the
428 nitrogen atom of the phenyl amine moiety, a common product within the oxidation pathway.
429 On the other hand, SMX-SO3H may be generated after hydroxylation followed by
430 fragmentation of the phenyl moiety. In the case of the SMX-NCN intermediate, three
431 secondary TPs were detected (SMX-Br-NCN, SMX-NO-NCN and SMX-NO2-NCN). SMX-Br-NCN is
432 a common intermediate in the halogenation pathway, formed by bromination of the
433 phenylamine nitrogen moiety. SMX-NO-NCN generation might be attributed to the oxidation
434 of the SMX-NCN phenylamine nitrogen to the nitrosobenzene group. Then, the generated
435 SMX-NO-NCN can be further oxidized from the nitrosobenzene group to nitrobenzene group,
436 forming the SMX-NO2-NCN intermediate.
437
438 As can be observed in Fig. 4A, Fig. 4B and Fig. 4C, primary halogenated TPs (SMX-Cl and SMX-
439 Br), dimeric 2SMX(-) TP, and oxidized TPs (SMX-OH, SMX-NCN and SMX-NO) presented their
440 maximum concentration at 120 min of sunlight irradiation, while secondary TPs accumulated
441 along the 6 hours of SMX degradation process. Detection of sulfamethoxazole intermediates

through different transformation pathways contributed to demonstrate the generation of RHS induced by solar irradiation of $TiO_2$ nanosized particles dispersed in seawater. Moreover, the proposed transformation mechanisms support the possible halogenation and dimerization of dissolved organic matter and micropollutants by photocatalytic treatments.

## Conclusions

Results presented in this work demonstrate the photogeneration of reactive halogen species through the irradiation of $TiO_2$ NPs with simulated sunlight in synthetic seawater. Selected scavenging tests and the identification of generated intermediates allowed the proposal of the $TiO_2$ photoactivation mechanism in this water matrix, this suggesting that RHS may result from the direct reactivity of halides with photogenerated holes. The efficiency of these active species in the degradation of organic pollutants, represented in this work by the model compound SMX, may be markedly slower compared with the reactive oxygen species generated in deionized water, which mainly involves hydroxyl radical oxidation. The photocatalytic SMX transformation in seawater occurred by halogenation, oxidation and dimerization as primary pathways, through reactions between this compound and the RHS generated in the $TiO_2$ photo-activation process. The evidence of RHS generation in the photocatalytic process studied in this work, brings concerns about the feasibility of photocatalytic water treatments using $TiO_2$ NPs in saline waters, as RHS could later lead to the generation and accumulation of potentially toxic compounds, such as halogenated and dimerized transformation products.

## Acknowledgements

This work was financially supported by MINECO/FEDER, UE (project CTQ2017-86466-R), Oriol Porcar's FPI fellowship (PRE2018-084184) and the agency for Management of University and Research Grants of the Government of Catalonia (project 2017SGR131).

## References

An, T., Yang, H., Li, G., Song, W., Cooper, W.J., Nie, X., 2010. Kinetics and mechanism of advanced oxidation processes (AOPs) in degradation of ciprofloxacin in water. Appl. Catal. B Environ. 94, 288–294. https://doi.org/10.1016/j.apcatb.2009.12.002

ASTM D1141-98, 2013. Standard for the Preparation of Substitute Ocean Water, ASTM International, West Conshohocken, PA, 2013. https://doi.org/10.1520/D1141-98R13

Bancirova, M., 2011. Sodium azide as a specific quencher of singlet oxygen during chemiluminescent detection by luminol and Cypridina luciferin analogues. Luminescence 26, 685–688. https://doi.org/10.1002/bio.1296

Bielski, B.H.J., Cabelli, D.E., Arudi, R.L., Ross, A.B., 1985. Reactivity of HO2/O2- Radicals in Aqueous Solution. J. Phys. Chem. Ref. Data 14, 1041–1100. https://doi.org/10.1063/1.555739

Borowska, E., Gomes, J.F., Martins, R.C., Quinta-Ferreira, R.M., Horn, H., Gmurek, M., 2019. Solar Photocatalytic Degradation of Sulfamethoxazole by TiO2 Modified with Noble Metals. Catalysts 9, 500.

Boutiti, A., Zouaghi, R., Bendjabeur, S.E., Guittonneau, S., Sehili, T., 2017. Photodegradation of 1-hexyl-3-methylimidazolium by UV/H2O2 and UV/TiO2: Influence of pH and chloride. J. Photochem. Photobiol. A Chem. 336, 164–169. https://doi.org/10.1016/j.jphotochem.2016.12.030

Bustos, N., Cruz-Alcalde, A., Iriel, A., Fernández Cirelli, A., Sans, C., 2019. Sunlight and UVC-254 irradiation induced photodegradation of organophosphorus pesticide dichlorvos in aqueous matrices. Sci. Total Environ. 649, 592–600. https://doi.org/10.1016/j.scitotenv.2018.08.254

Buxton, G. V., Greenstock, C.L., Helman, W.P., Ross, A.B., 1988. Critical Review of rate constants for reactions of hydrated electrons, hydrogen atoms and hydroxyl radicals

(·OH/·O−) in Aqueous Solution. J. Phys. Chem. Ref. Data 17, 513–886. https://doi.org/10.1063/1.555805

Byrne, C., Subramanian, G., Pillai, S.C., 2018. Recent advances in photocatalysis for environmental applications. J. Environ. Chem. Eng. 6, 3531–3555. https://doi.org/10.1016/j.jece.2017.07.080

Cai, Q., Hu, J., 2017. Decomposition of sulfamethoxazole and trimethoprim by continuous UVA/LED/TiO2 photocatalysis: Decomposition pathways, residual antibacterial activity and toxicity. J. Hazard. Mater. 323, 527–536. https://doi.org/10.1016/j.jhazmat.2016.06.006

Catalán, J., Díaz, C., Barrio, L., 2004. Analysis of mixed solvent effects on the properties of singlet oxygen (1Δg). Chem. Phys. 300, 33–39. https://doi.org/10.1016/j.chemphys.2004.01.010

Cavalcante, R.P., Dantas, R.F., Bayarri, B., González, O., Giménez, J., Esplugas, S., Machulek, A., 2016. Photocatalytic mechanism of metoprolol oxidation by photocatalysts TiO2 and TiO2 doped with 5% B: Primary active species and intermediates. Appl. Catal. B Environ. 194, 111–122. https://doi.org/10.1016/j.apcatb.2016.04.054

D. Camacho-Muñoz, L.L. and C.E., 2020. Degradation of okadaic acid in seawater by UV/TiO2 photocatalysis – Proof of concept. Sci. Total Environ. https://doi.org/10.1016/j.colsurfa.2020.124658

Daimon, T., Hirakawa, T., Kitazawa, M., Suetake, J., Nosaka, Y., 2008. Formation of singlet molecular oxygen associated with the formation of superoxide radicals in aqueous suspensions of TiO2 photocatalysts. Appl. Catal. A Gen. 340, 169–175. https://doi.org/10.1016/j.apcata.2008.02.012

Dodd, M.C., Huang, C.H., 2004. Transformation of the antibacterial agent sulfamethoxazole in reactions with chlorine: Kinetics, mechanisms, and pathways. Environ. Sci. Technol. 38, 5607–5615. https://doi.org/10.1021/es035225z

Doudrick, K., Yang, T., Hristovski, K., Westerhoff, P., 2013. Photocatalytic nitrate reduction in water: Managing the hole scavenger and reaction by-product selectivity. Appl. Catal. B Environ. 136–137, 40–47. https://doi.org/10.1016/j.apcatb.2013.01.042

Fotiou, T., Triantis, T.M., Kaloudis, T., O'Shea, K.E., Dionysiou, D.D., Hiskia, A., 2016. Assessment of the roles of reactive oxygen species in the UV and visible light photocatalytic degradation of cyanotoxins and water taste and odor compounds using C-TiO2. Water Res. 90, 52–61. https://doi.org/10.1016/j.watres.2015.12.006

Fujishima, A., Zhang, X., Tryk, D.A., 2008. TiO2 photocatalysis and related surface phenomena. Surf. Sci. Rep. 63, 515–582. https://doi.org/10.1016/j.surfrep.2008.10.001

Gao, S., Zhao, Z., Xu, Y., Tian, J., Qi, H., Lin, W., Cui, F., 2014. Oxidation of sulfamethoxazole (SMX) by chlorine, ozone and permanganate-A comparative study. J. Hazard. Mater. 274, 258–269. https://doi.org/10.1016/j.jhazmat.2014.04.024

García-Fernández, I., Fernández-Calderero, I., Inmaculada Polo-López, M., Fernández-Ibáñez, P., 2015. Disinfection of urban effluents using solar TiO2 photocatalysis: A study of significance of dissolved oxygen, temperature, type of microorganism and water matrix. Catal. Today 240, 30–38. https://doi.org/10.1016/j.cattod.2014.03.026

Grebel, J.E., Pignatello, J.J., Song, W., Cooper, W.J., Mitch, W.A., 2009. Impact of halides on the photobleaching of dissolved organic matter. Mar. Chem. 115, 134–144. https://doi.org/10.1016/j.marchem.2009.07.009

Hao, Z., Yin, Y., Wang, J., Cao, D., Liu, J., 2018. Formation of organobromine and organoiodine compounds by engineered TiO2 nanoparticle-induced photohalogenation of dissolved organic matter in environmental waters. Sci. Total Environ. 631–632, 158–168. https://doi.org/10.1016/j.scitotenv.2018.03.027

Jedsukontorn, T., Ueno, T., Saito, N., Hunsom, M., 2018. Mechanistic aspect based on the role of reactive oxidizing species (ROS) in macroscopic level on the glycerol photooxidation over defected and defected-free TiO2. J. Photochem. Photobiol. A Chem. 367, 270–281.

https://doi.org/10.1016/j.jphotochem.2018.08.030

Jiang, J., Zhang, X., Zhu, X., Li, Y., 2017. Removal of Intermediate Aromatic Halogenated DBPs by Activated Carbon Adsorption: A New Approach to Controlling Halogenated DBPs in Chlorinated Drinking Water. Environ. Sci. Technol. 51, 3435–3444. https://doi.org/10.1021/acs.est.6b06161

Liu, J., Zhang, X., 2014. Comparative toxicity of new halophenolic DBPs in chlorinated saline wastewater effluents against a marine alga: Halophenolic DBPs are generally more toxic than haloaliphatic ones. Water Res. 65, 64–72. https://doi.org/10.1016/j.watres.2014.07.024

Mahmoud, W.M.M., Rastogi, T., Kümmerer, K., 2017. Application of titanium dioxide nanoparticles as a photocatalyst for the removal of micropollutants such as pharmaceuticals from water. Curr. Opin. Green Sustain. Chem. 6, 1–10. https://doi.org/10.1016/j.cogsc.2017.04.001

Martins, R.C., Domingues, E., Bosio, M., Quina, M.J., Gmurek, M., Quinta-ferreira, R.M., Gomes, J., 2019. Effect of Different Radiation Sources and Noble Metal Doped onto TiO2 for Contaminants of Emerging Concern Removal. Water 11, 894. https://doi.org/10.3390/w11050894

Nosaka, Y., Nosaka, A.Y., 2017. Generation and Detection of Reactive Oxygen Species in Photocatalysis. Chem. Rev. 117, 11302–11336. https://doi.org/10.1021/acs.chemrev.7b00161

Riaz, S., Park, S.J., 2020. An overview of TiO2-based photocatalytic membrane reactors for water and wastewater treatments. J. Ind. Eng. Chem. 84, 23–41. https://doi.org/10.1016/j.jiec.2019.12.021

Ribao, P., Corredor, J., Rivero, M.J., Ortiz, I., 2019. Role of reactive oxygen species on the activity of noble metal-doped TiO2 photocatalysts. J. Hazard. Mater. 372, 45–51. https://doi.org/10.1016/j.jhazmat.2018.05.026

Rodríguez, E.M., Márquez, G., Tena, M., Álvarez, P.M., Beltrán, F.J., 2014. Determination of main species involved in the first steps of TiO2 photocatalytic degradation of organics with the use of scavengers: The case of ofloxacin. Appl. Catal. B Environ. 178, 44–53. https://doi.org/10.1016/j.apcatb.2014.11.002

Romero-Martínez, L., Moreno-Andrés, J., Acevedo-Merino, A., Nebot, E., 2014. Improvement of ballast water disinfection using a photocatalytic (UV-C + TiO2) flow-through reactor for saltwater treatment. J. Chem. Technol. Biotechnol. 89, 1203–1210. https://doi.org/10.1002/jctb.4385

Rubio, D., Casanueva, J.F., Nebot, E., 2013. Improving UV seawater disinfection with immobilized TiO2: Study of the viability of photocatalysis (UV254/TiO2) as seawater disinfection technology. J. Photochem. Photobiol. A Chem. 271, 16–23. https://doi.org/10.1016/j.jphotochem.2013.08.002

Tiwari, A., Shukla, A., Lalliansanga, Tiwari, D., Lee, S.M., 2019. Au-nanoparticle/nanopillars TiO2 meso-porous thin films in the degradation of tetracycline using UV-A light. J. Ind. Eng. Chem. 69, 141–152. https://doi.org/10.1016/j.jiec.2018.09.027

von Sonntag, C., von Gunten, U., 2012. Chemistry of Ozone in Water and Wastewater Treatment: From Basic Principles to Applications, IWA Publishing. https://doi.org/10.2166/9781780400839

Xiao, J., Xie, Y., Han, Q., Cao, H., Wang, Y., Nawaz, F., Duan, F., 2016. Superoxide radical-mediated photocatalytic oxidation of phenolic compounds over Ag+/TiO2: Influence of electron donating and withdrawing substituents. J. Hazard. Mater. 304, 126–133. https://doi.org/10.1016/j.jhazmat.2015.10.052

Yuan, R., Zhu, Y., Zhou, B., Hu, J., 2019. Photocatalytic oxidation of sulfamethoxazole in the presence of TiO2: Effect of matrix in aqueous solution on decomposition mechanisms. Chem. Eng. J. 359, 1527–1536. https://doi.org/10.1016/j.cej.2018.11.019

Zhang, K., Parker, K.M., 2018. Halogen Radical Oxidants in Natural and Engineered Aquatic

Systems. Environ. Sci. Technol. 52, 9579–9594. https://doi.org/10.1021/acs.est.8b02219

Zhang, Y., Li, J., Bai, J., Li, L., Xia, L., Chen, S., Zhou, B., 2017. Dramatic enhancement of organics degradation and electricity generation via strengthening superoxide radical by using a novel 3D AQS/PPy-GF cathode. Water Res. 125, 259–269. https://doi.org/10.1016/j.watres.2017.08.054

Zheng, S., Cai, Y., O'Shea, K.E., 2010. TiO2 photocatalytic degradation of phenylarsonic acid. J. Photochem. Photobiol. A Chem. 210, 61–68. https://doi.org/10.1016/j.jphotochem.2009.12.004

# Supplementary information

## Photocatalytic degradation of sulfamethoxazole using $TiO_2$ in simulated seawater: evidence for direct formation of reactive halogen species and halogenated by-products

Oriol Porcar-Santos*, Alberto Cruz-Alcalde, Núria López-Vinent, Dimitrios Zanganas, Carme Sans

Department of Chemical Engineering and Analytical Chemistry, Faculty of Chemistry, Universitat de Barcelona, C/Martí i Franqués 1, 08028 Barcelona, Spain.

*Corresponding author: oriol.porcar@ub.edu

**List of supplementary data:**


| Content | Title | Page |
|---|---|---|
| Table S1 | Concentrations of the different salts added for the seawater preparation | 2 |
| Figure S1 | Scan of the detected intermediate SMX-Br (329.96-331.96 m/z) with its fragmented ion of 233.92-235.92 m/z by negative electrospray ionization | 2 |
| Figure S2 | Scan of the detected intermediate SMX-NO (266.03 m/z) with its fragmented ion of 169.99 m/z by negative electrospray ionization | 3 |
| Figure S3 | Scan of the detected intermediate SMX-OH (268.04 m/z) with its fragmented ion of 172.01 m/z by negative electrospray ionization | 3 |
| Figure S4 | Scan of the detected intermediate SMX-NO2 (282.02 m/z) with its fragmented ion of 185.99 m/z by negative electrospray ionization | 4 |


**Table S1.** Concentrations of the different salts added for the seawater preparation

| Salts | Concentration (g/L) |
|---|---|
| NaCl | 24.530 |
| $MgCl_2$ | 5.200 |
| $Na_2SO_4$ | 4.090 |
| $CaCl_2$ | 1.160 |
| KCl | 0.695 |
| $NaHCO_3$ | 0.201 |
| KBr | 0.101 |
| $H_3BO_3$ | 0.027 |

**Figure S1.** Scan of the detected intermediate SMX-Br (329.96-331.96 m/z) with its fragmented ion of 233.92-235.92 m/z by negative electrospray ionization

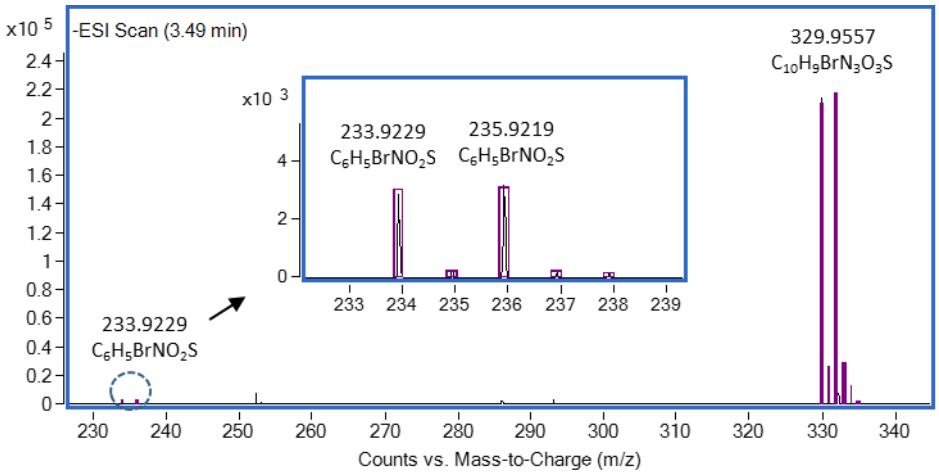

**Figure S2.** Scan of the detected intermediate SMX-NO (266.03 m/z) with its fragmented ion of 169.99 m/z by negative electrospray ionization

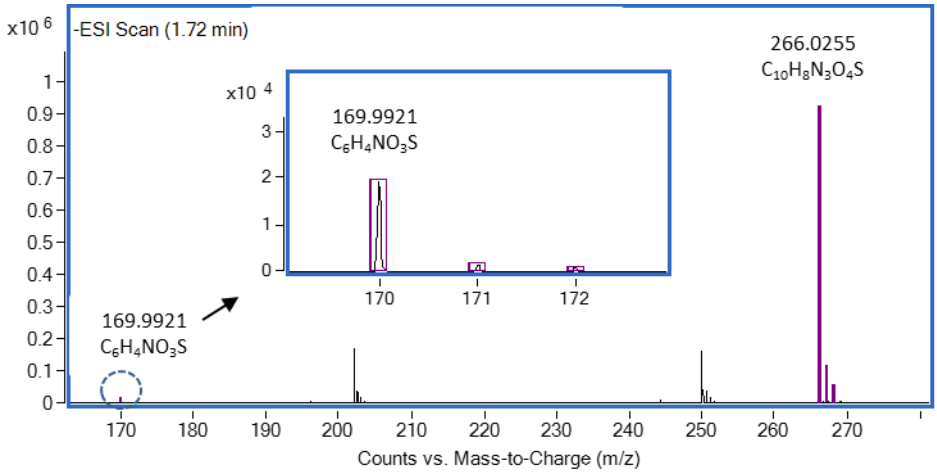


**Figure S3.** Scan of the detected intermediate SMX-OH (268.04 m/z) with its fragmented ion of 172.01 m/z by negative electrospray ionization

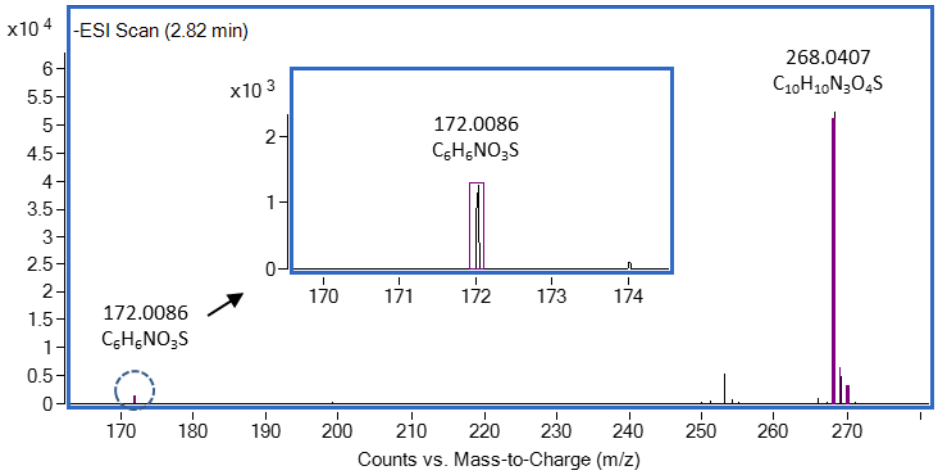

674

675 **Figure S4.** Scan of the detected intermediate SMX-NO2 (282.02 m/z) with its fragmented ion of
676 185.99 m/z by negative electrospray ionization

677

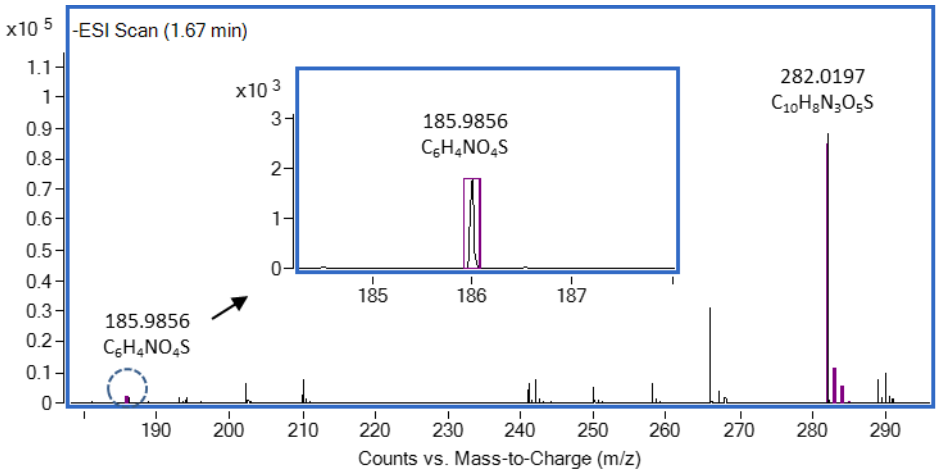


678

679